Numerical Analysis of Traveling-Wave Photodetectors' Bandwidth Using the Finite-Difference Time-Domain Method

Soon-Cheol Kong, Seung-Jin Lee, Jung-Hoon Lee, and Young-Wan Choi, *Member, IEEE*

***Abstract*—We present full-wave analysis of traveling-wave photodetectors (TWPDs) using the finite-difference time-domain (FDTD) method. Impulse response in the frequency domain is obtained after time-domain data are calculated by the FDTD method. The impulse response includes the optical field profile, carrier transit time, microwave loss, microwave dispersion, and velocity mismatch all together. Three-decibel bandwidth is analyzed with the thickness of an i-layer and waveguide width as the design parameters. It is shown how transit time and microwave characteristics affect the bandwidth according to the TWPD's length. Three-decibel bandwidth is dominated by carrier transit time in case the device length is shorter than 300–500 μm under the conditions given in this paper. However, if the device length gets longer, microwave characteristics affect the bandwidth.**

***Index Terms*—Finite-difference time-domain (FDTD) method, RF optic link, traveling-wave photodetector (TWPD).**

I. Introduction

RESEARCH ON millimeter-wave photonics will contribute to communication service where wired and wireless systems are integrated. In such integrated systems, an ultrawide-band and efficient photodetector such as a traveling-wave photodetector (TWPD) would be an essential component.

The concept of a traveling-wave device was first suggested by Soohoo *et al.* in 1981 [1] and the TWPD was reported by Taylor *et al.* in 1990 [2] to get over the limitation of bandwidth efficiency product of conventional lumped-type photodetectors. The TWPD can be utilized with other optical waveguide devices [3], and it can especially be integrated with a semiconductor optical amplifier [4]. In general, the TWPD's characteristic impedance is matched to the output port and, consequently, only a traveling wave exists in the device without a reflected wave. A peculiar characteristic of the TWPD is the fact that the bandwidth of the TWPD is limited by the optical-absorption-coefficient velocity mismatch, not by an *RC* time constant [5], which impedance matching to the load circuit can eliminate. A velocity-matched p-i-n TWPD was reported in [6]. Some papers showed impulse responses resulted from velocity mismatch, considering the input facet as an open or matched termination. However, these papers did not take into account microwave loss together [5], [7].

A high bandwidth-efficiency product and high saturation output current are important aspects in the study of high-speed photodetectors. Microwave loss limits the bandwidth of TWPDs in the case of high-power photodetectors because they need long device length (hundreds of micrometers) and a low modal optical absorption coefficient. This paper focuses on the bandwidth-limiting factors according to the device length and the tradeoff between the bandwidth and output current.

Most of the studies on TWPDs have been done by the equivalent-circuit model, in which the inductance value of a ridge-type coplanar waveguide (CPW) (hybrid coplanar) approximates to that of a planar CPW. However, this calculation uses a geometrical factor and, therefore, it limits the device type for exact simulation. Especially in a case that the distance between the signal electrode and ground electrode increases, it is difficult to consider fringing fields and to define the type of TWPD (microstrip or CPW).

In this paper, analysis is carried out using the finite-difference time-domain (FDTD) method [8]. This method is a numerical analysis technique that discretizes the Maxwell's equations; thereby any complicated structure can be simulated easily without treating a special boundary condition for material because the constitute parameters (ϵ, μ, σ) reflect the material property and the configuration of the device. For that reason, a ridge-type CPW TWPD of multilayered structure can be analyzed exactly considering microwave loss, dispersion, and velocity mismatch by the FDTD method. In [9] and [10], full-wave analyses of photoconductive switches have been studied using a self-consistent FDTD modeling with a charge transport.

The source modeling is applied to the numerical simulation considering the photocurrent that is generated in the active i-layer when an optical signal propagates. We also derived a formula for source modeling and applied it to the FDTD method to take into account the carrier transit time. To the best of our knowledge, this kind of study has not yet been tried. The characteristic impedance was also calculated by the Agilent High Frequency Structure Simulator (HFSS) and the results were compared with those attained by the FDTD method to validate our simulation results. However, only our FDTD

Manuscript received August 6, 2001; revised October 20, 2001.

S.-C. Kong is with the Optoelectronics and Optical Communications Laboratory, Chung-Ang University, Seoul 156-756, Korea.

S.-J. Lee was with the Optoelectronics and Optical Communications Laboratory, Chung-Ang University, Seoul 156-756, Korea. He is now with Samsung Electronics, Suwon 442-742, Korea.

J.-H. Lee was with the Optoelectronics and Optical Communications Laboratory, Chung-Ang University, Seoul 156-756, Korea. He is now with Blue Stellar Wave, Inchon 470-050, Korea.

Y.-W. Choi is with the Department of Electronic Engineering, Chung-Ang University, Seoul 156-756, Korea.

Digital Object Identifier 10.1109/TMTT.2002.804508

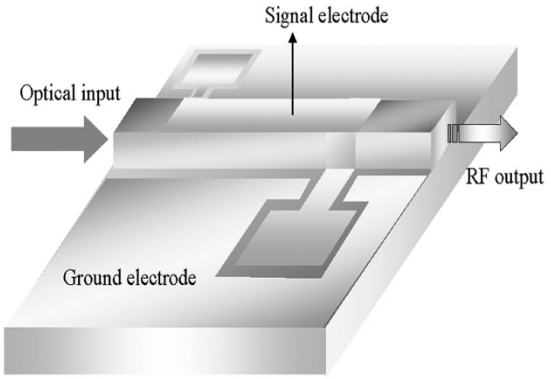

(a)

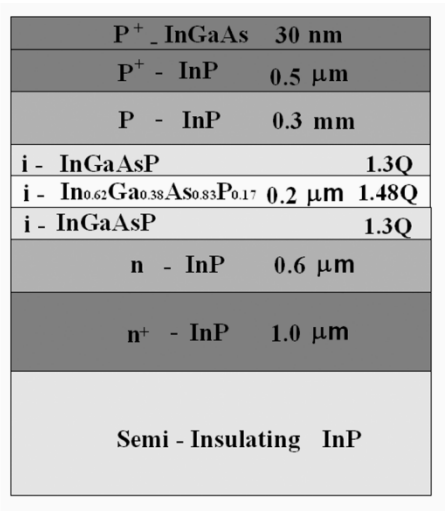

(b)

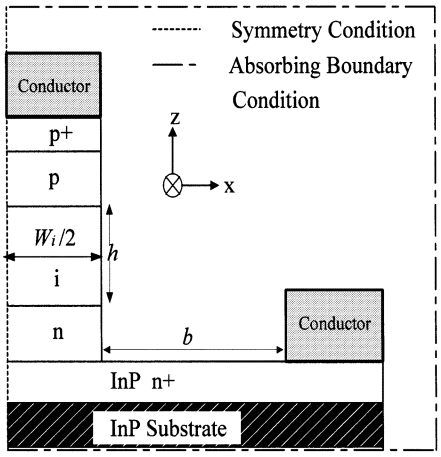

(c)

Fig. 1. (a) TWPD structure with electrodes for dc bias. (b) Cross-sectional layer structure of the TWPD. (c) xz-plane view of the TWPD used in the FDTD simulation ($b = 5.7$ μm).

simulation can obtain an impulse response considering the propagation of both the optical wave and microwave because the HFSS software calculates just the microwave property.

It will be shown that a broader bandwidth can be obtained in TWPDs with a lower microwave loss and enhanced microwave velocity in case of an open input facet, and that impedance matching can be achieved by proper design of cross-sectional geometry.

II. Device Structure and FDTD Formulation

We consider a layer structure of a ridge-type traveling-wave coplanar waveguide (TW CPW) photodetector (bulk) on a semi-insulating InP substrate for 1.55-μm operation, as shown in Fig. 1. Intrinsic $In_{0.62}Ga_{0.38}As_{0.83}P_{0.17}$ ($\lambda_g = 1.485$ μm) active region (0.2-μm thickness) is sandwiched by undoped InGaAsP (1.3Q) layers. InP is used for the p- and n-type contact layers.

The FDTD method solves the Maxwell's curl equations directly. Yee's mesh [8] is used to accommodate the detailed configuration of our device structure. Since the divergence equations

TABLE I
Constitutive Parameters That Are Used in the Simulations ($\mu_r = 1.0$ for All Layers)

	Relative Permittivity (ϵ_r)	Conductivity (σ) [S/m]
Center Conductor (Gold)	1.0	4.1×10^7
P+	12.4	20000
P	13.26	1980
I	Active region : 12.38 Cladding region : 11.55	0
N	13.26	24000
N+	12.4	560000
Substrate	12.4	0

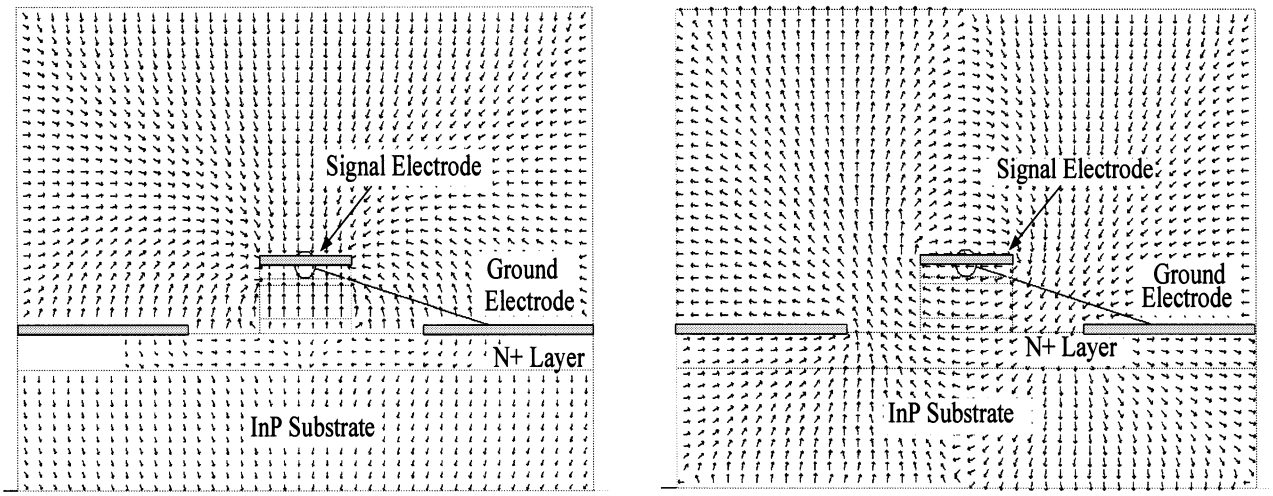

(a) (b)

Fig. 2. Microwave fields distribution (log scale) on a cross section of the output port calculated by HFSS. (a) Electric field. (b) Magnetic field.

are not independent, we just need the following two equations:

$$\nabla \times \bar{E} = -\frac{\partial \bar{B}}{\partial t} \tag{1}$$

$$\nabla \times \bar{H} = \frac{\partial \bar{D}}{\partial t} + \bar{J}. \tag{2}$$

The differential equations are discretized for simulation coding of our geometry, and the electric and magnetic fields are calculated in both the time and space domains. As the field components are governed by Maxwell's equations, the three-dimensional (3-D) multilayered structure is considered completely with the constitutive parameters (permittivity, permeability, and conductivity). To ensure stability of the FDTD algorithm, the Courant condition is applied [11] and Mur's absorbing boundary condition [12] is used to simulate the propagation of outgoing waves on the outer boundary, as shown in Fig. 1(c).

Fig. 1(c) shows the cross section of the TWPD in the xz-plane. Both optical wave and microwave propagate in the y-direction. Taking advantage of the lateral symmetry, only the half-space is used for numerical simulation and, therefore, the memory requirements and calculation time are reduced. The magnetic wall ($H_y = H_z = 0$) is applied on the yz-plane as a symmetry condition. The material constitutive parameters used in the simulations are listed in Table I. The conductor's thickness was set to 0.5 μm in all simulations. In the conductive media, the conductivity is given by $\sigma = q\,(\mu_n n + \mu_p p)$, which incorporates the doping concentrations of the material and the skin effect into the simulation. In the intrinsic and substrate layers, the conductivity is assumed to be zero.

The distance between the signal and ground electrodes ($b = 5.7\,\mu$m) and the ground electrode width (=6.3 μm) in Fig. 1(b) are fixed for all simulations. The space steps used are $\Delta x = 0.3\,\mu$m, $\Delta y =$ device length/15, and $\Delta z = 0.1\ \mu$m, and the total mesh dimensions are $50 \times 59 \times 65$ in the x-, y-, and z-directions, respectively. Also, the time increment (Δt) used is 0.2 fs.

The simulated results presented in this paper are divided into two classes. One is the response of the optical impulse and the other is the characteristic of the microwave.

A. Source Modeling for Impulse Response

A TWPD has optical power input and microwave current output and, therefore, we need a source modeling for FDTD simulation to get an impulse response. The optical power absorbed per unit length at any point along the detector is $P_{\rm abs}(y) = -d|P(y)|/dy = \Gamma\alpha_0 P_0 e^{-\Gamma\alpha_0 y}$, where Γ is the optical confinement factor, α_0 is the power absorption coefficient, and P_o is the incident optical power. For a source modeling of the optical impulse response, we regard photogenerated current density as a produced conductivity by photogenerated carriers. $J_z(y)$ can then be written as $\sigma E_z(y) = q(\mu_n n + \mu_p p)E_z(y) \approx q\mu_n n E_z(y) = q v_{\rm sat} n$, where q is the elementary charge and $v_{\rm sat}$ is the carrier saturation velocity. To derive a formula for a current density source, we let $J_z(y)/q$ [(# of EHP)/(s $\cdot$ A)] equal $(\lambda/hc)(P_{\rm abs}(y)/W_i)$ [(# of photons)/(s $\cdot$ A)] with η_i (the internal quantum efficiency) $= 1$, where λ is the optical wavelength, h is the Plank constant, and W_i is the waveguide width. The current density can then be written as

$$J_z(y) = \frac{q\lambda}{hcW_i}\Gamma\alpha_0 P_0 e^{-\Gamma\alpha_0 y}. \tag{3}$$

The validation of (3) can be identified by taking the surface integral of J_z. That is to say, $I_{\rm photo} = \int_0^{\rm DL}\int_0^{W_i} J_z(y)dxdy$ yields $P_0 q\lambda(1 - e^{-\Gamma\alpha_0 \rm DL})/hc$ as expected, where DL denotes the device length.

For a practical application of (3) to consider the carrier transit time, the photocurrent [A/m^2] in the i-layer at $t = n\Delta t$ (n is the time-step index) is expressed as follows:

$$J_z^n(i,j,k) = x_{\rm profile}[i] n_x z_{\rm profile}\left[\frac{n - t_{\rm opt}[j] - t_1}{(t_2 - t_1)/n_z}\right] \times \frac{1}{(t_2 - t_1)/n_z}\frac{q\lambda}{hcW_i}\Gamma\alpha_o P_o e^{-\Gamma\alpha_O j\Delta y} \tag{4a}$$

$$\mathrm{ofp}(i,k) = x_{\rm profile}[i] \times z_{\rm profile}[k] \tag{4b}$$

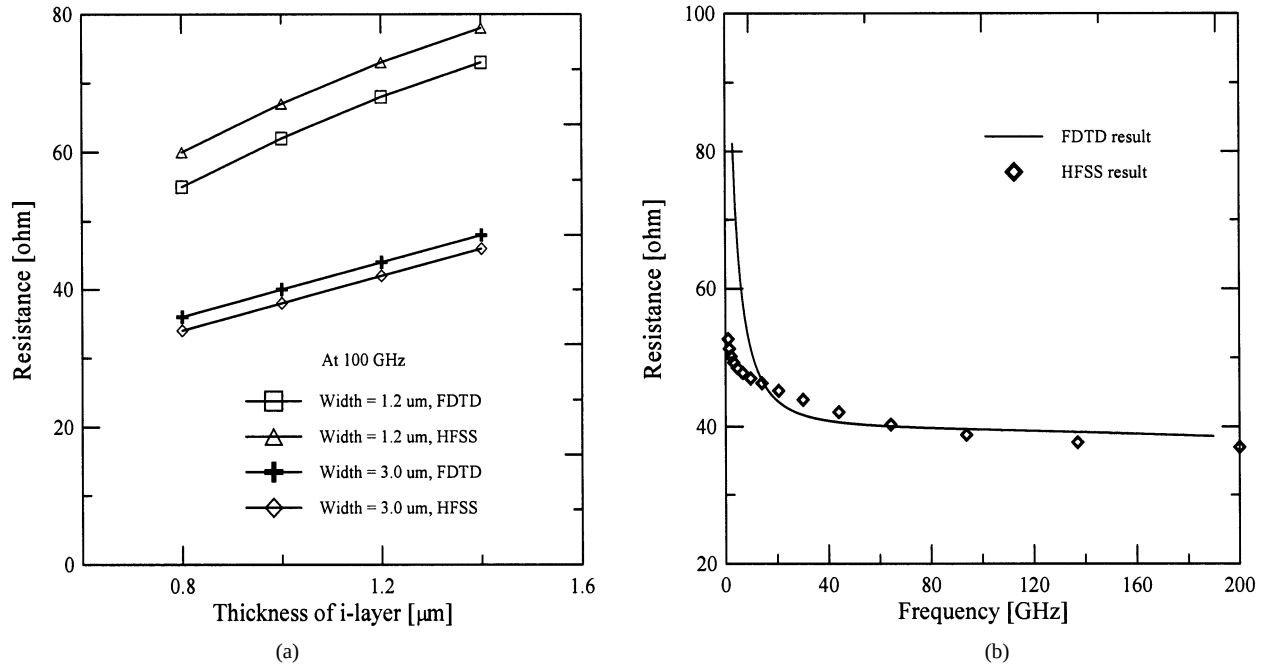

Fig. 3. Real part of characteristic impedance. (a) At 100 GHz with the waveguide widths of 1.2 and 3.0 μm according to the thickness of the i-layer. (b) With the waveguide width of 3.0 μm and the thickness of the i-layer of 1.0 μm as a function of frequency. The results were attained by FDTD and HFSS simulations.

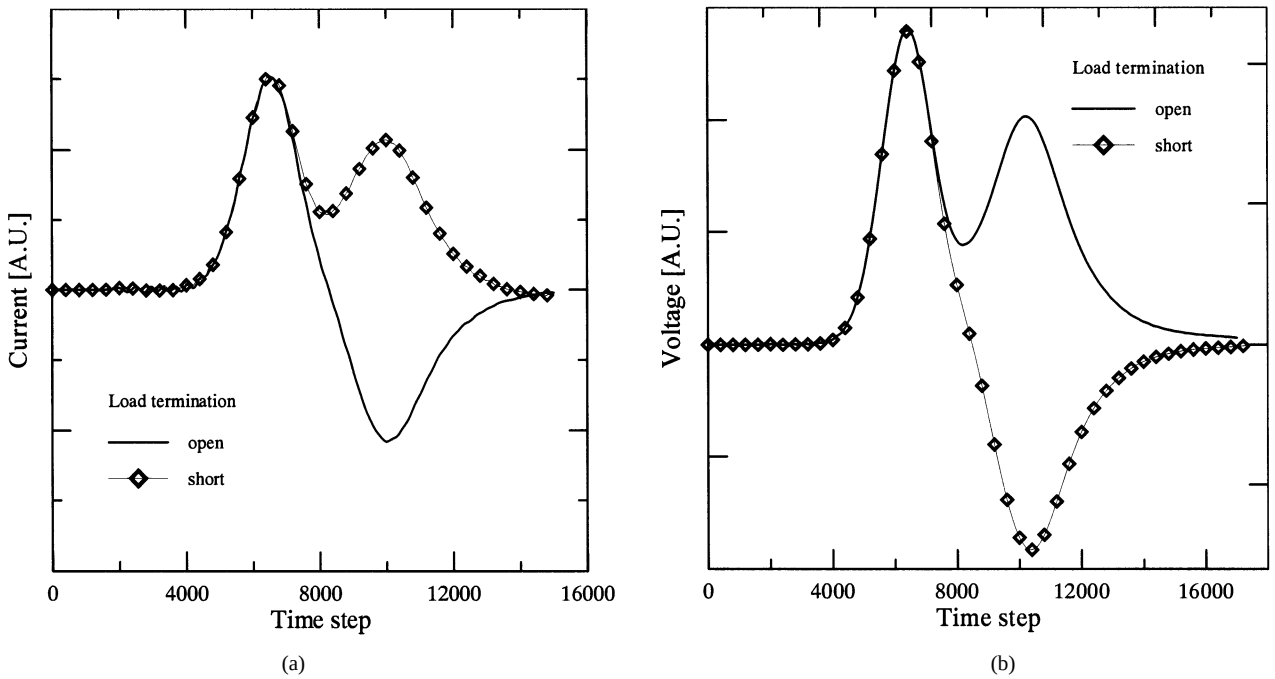

Fig. 4. Signals as simulated by the FDTD method in the time domain ($W_i = 3.0$ μm, $h = 1.0$ μm, time step $= 0.2$ fs). (a) Current with open and short load termination. (b) Voltage with open and short load termination.

where i, j, and k are integer indexes of the x, y, and z-axes respectively, and n_x is defined as $W_i/\Delta x$. Here, it is assumed that the photogenerated carriers drift across the i-layer with the saturation velocity and that the output terminal is impedance matched regardless of the characteristic impedance of the TWPD. Thus, there exists only a traveling wave, and in the RF optic link communication system, the output can be matched to the next circuit using an impedance transformer. We define $t_1 \times \Delta t$ and $t_2 \times \Delta t$ as the carrier drift time to reach the conductive media (Δt is the time increment in the FDTD simulation) from the top and bottom active i-layer, respectively, and photoabsorption layer thickness as d. Saturation velocity is then $v_{\rm sat} = d/\{\Delta t(t_2 - t_1)\}$. Also, $1/v_{\rm sat}^4 = (1/v_e^4 + 1/v_h^4)/2$, where v_e and v_h are the electron and hole velocities, is used [13]. In (4a), the photogenerated carriers in the intrinsic region are expressed as the current density, which can be applied into (2) for $(t_{\rm opt}[j]+t_1)\Delta t \leqq t \leqq (t_{\rm opt}[j]+t_2)\Delta t$. Here, $t_{\rm opt}[j]\Delta t$ is the time for the incident optical signal to reach a position

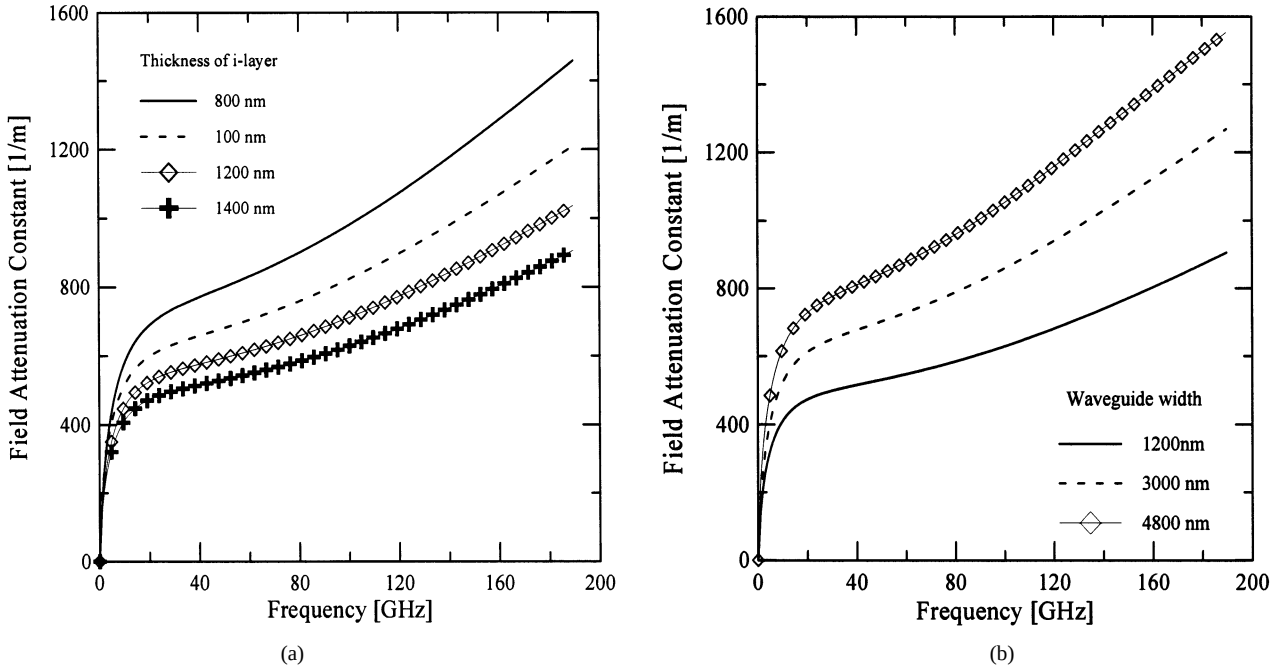

Fig. 5. Field attenuation constant with the parameter of the: (a) thickness of the i-layer ($W_i = 1.2\ \mu$m) and (b) waveguide width ($h = 1.4\ \mu$m).

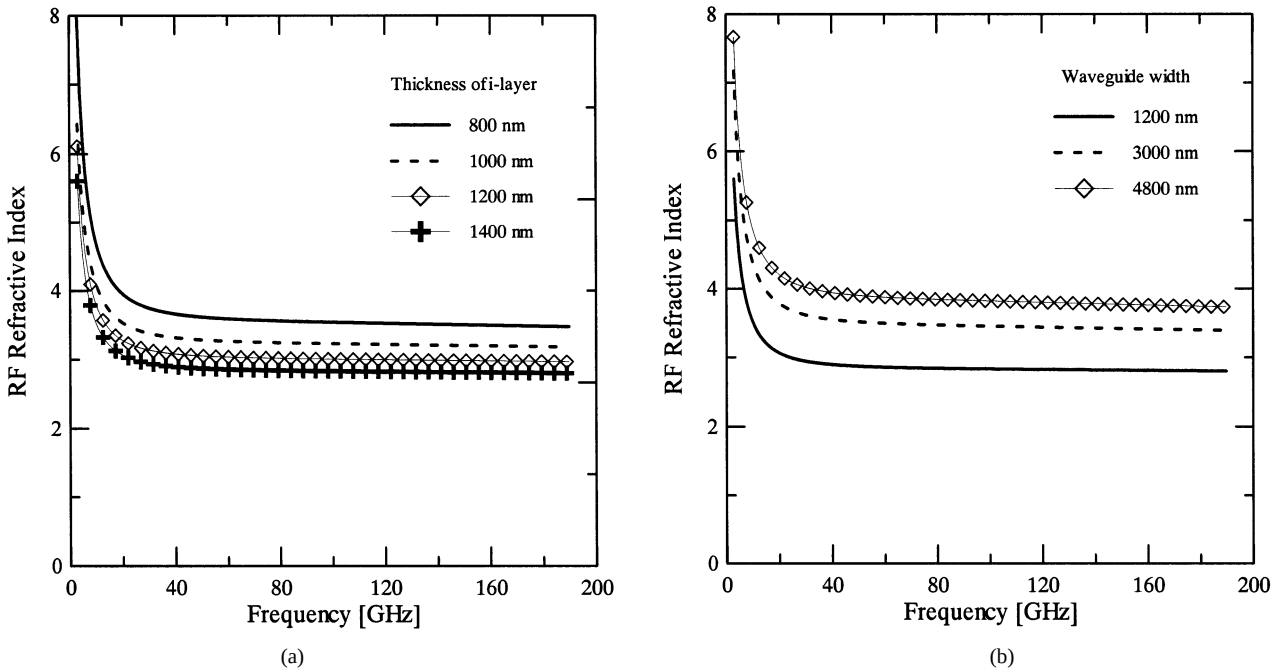

Fig. 6. RF refractive index with the parameter of the : (a) thickness of the i-layer ($W_i = 1.2\ \mu$m) and (b) waveguide width ($h = 1.4\ \mu$m).

$(y = j\Delta y)$ from the input end at optical group velocity. In (4b), $\mathrm{ofp}(i,k)$ is the optical field profile in the xz-plane calculated by the effective index method [14]. In this study, the 100-array elements of $z_{\mathrm{profile}}[k]$, which are z-position dependent in (4b), are applied into (4a) as a function of time. Thus, the transit time effect is considered in the source modeling of the FDTD code.

Since the higher efficiency helps relieve the burden imposed on millimeter-wave components and also makes their integration easier, the input facet of the waveguide is open terminated in the impulse response simulations. This makes high efficiency with 100% reflection at the input end, and the bandwidth-efficiency product with open-circuit input termination is generally larger than with a matched input termination [5].

B. Microwave Characteristics

We use a Gaussian pulse as an excitation of the input signal to evaluate the broad-band microwave behavior. We obtained the frequency-domain parameters by Fourier transforming the data obtained in the time domain. The structure of the TWPD guides the optical signal and also plays the role of the microwave transmission line. The following equations were used to calculate the

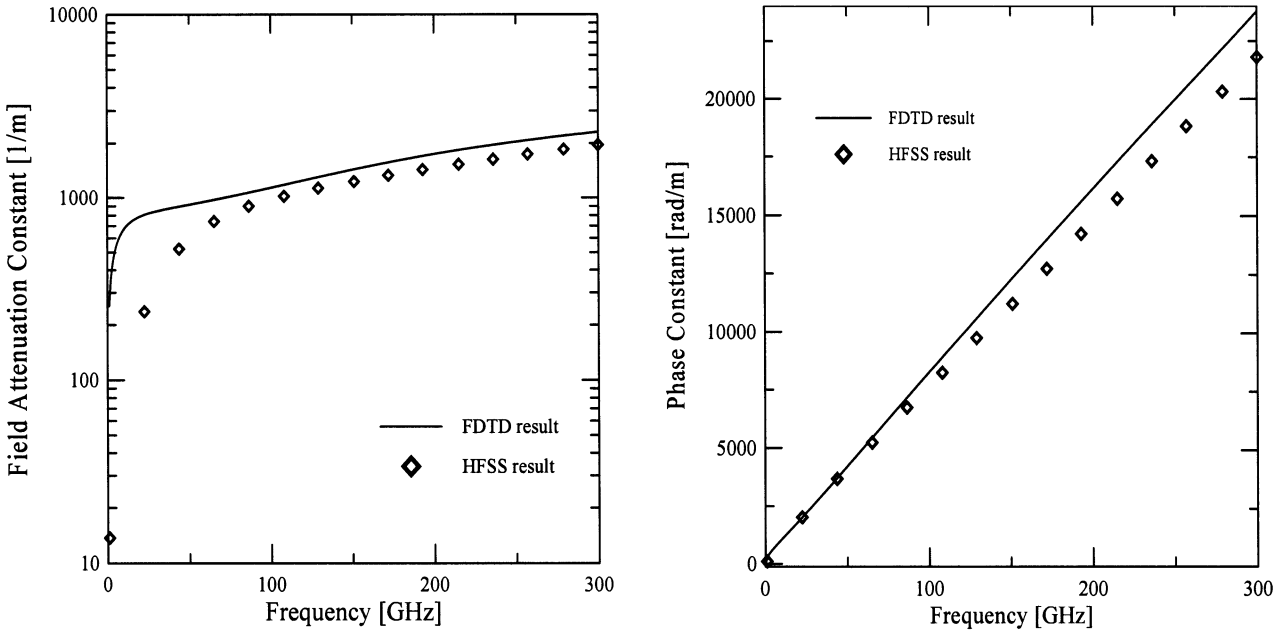

(a) (b)

Fig. 7. (a) Field attenuation constant. (b) Phase constant ($W_i = 3.0\ \mu$m, $h = 1.0\ \mu$m).

microwave characteristic impedance and propagation constant. They are easily derived from the transmission-line equations

$$Z_c(f, y_i) = \sqrt{Z_{\rm open}(f, y_i) \times Z_{\rm short}(f, y_i)} \tag{5}$$

$$\gamma(f, y_i) = \frac{1}{l} \tanh^{-1} \sqrt{\frac{Z_{\rm short}(f, y_i)}{Z_{\rm open}(f, y_i)}}. \tag{6}$$

Here, $Z_{\rm open}$ and $Z_{\rm short}$ are the input impedances (at the position of y_i) of a TWPD with open and short termination, respectively, and l is the distance between the load and field observation position (y_i). The input impedance with open- or short-output termination is calculated by applying $Z(f, y_i) = \mathcal{F}[V(t, y_i)]/\mathcal{F}[I(t, y_i)]$, where $\mathcal{F}$ denotes the Fourier-transform operator. The electric and magnetic walls are enforced on the device-output plane for short and open conditions, respectively. Voltages and currents in the time domain are obtained by taking the line integral of the electric field between the center conductor and ground electrode, and by taking the closed integral of the magnetic field around the center conductor, respectively. Liang *et al.* analyzed the case of a CPW and slotline by applying (5) and (6) in [15].

III. Results and Discussions

The FDTD simulation enables us to consider transit-time effect, optical-field profile, microwave loss, microwave dispersion, and velocity mismatch all together. The i-layer material optical power-absorption coefficient used in the simulation is 1000 cm^{-1}. We analyzed with two parameters the thickness of the i-layer and the waveguide width (h and W_i in Fig. 1). From (6), we obtained the propagation constant $(\gamma = \alpha + j\beta)$, and its real and imaginary terms represent microwave loss and dispersion, respectively.

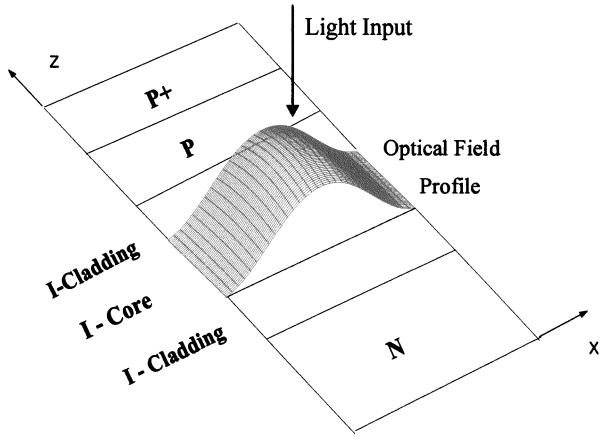

Fig. 8. Optical field distribution in the intrinsic active region for source modeling of the TWPD's input signal.

Electric- and magnetic-field distributions are shown in Fig. 2. The simulation was executed by Agilent HFSS (version 5.6), which uses the finite-element method (FEM) as a numerical technique.[1] The lengths of arrows are plotted in a log scale. The figures show that the n+ layer almost blocks the electric field, but the magnetic field penetrates the n+ and substrate region. The real parts of the characteristic impedance values calculated by both the FDTD method and HFSS are compared in Fig. 3. The waveguide width was set to 1.2 and 3.0 μm in the simulation of Fig. 3(a) and the results were obtained at a frequency of 100 GHz. Only the resistances are shown because the reactance values are close to zero. Fig. 3(b) shows the characteristic impedance as a function of frequency. High resistance can be achieved by having a narrow waveguide width and a deep thickness of the i-layer, and 50-Ω output-impedance matching can be

[1]*Agilent HFSS 5.6.*, Agilent Technol., Palo Alto, CA, 2000.

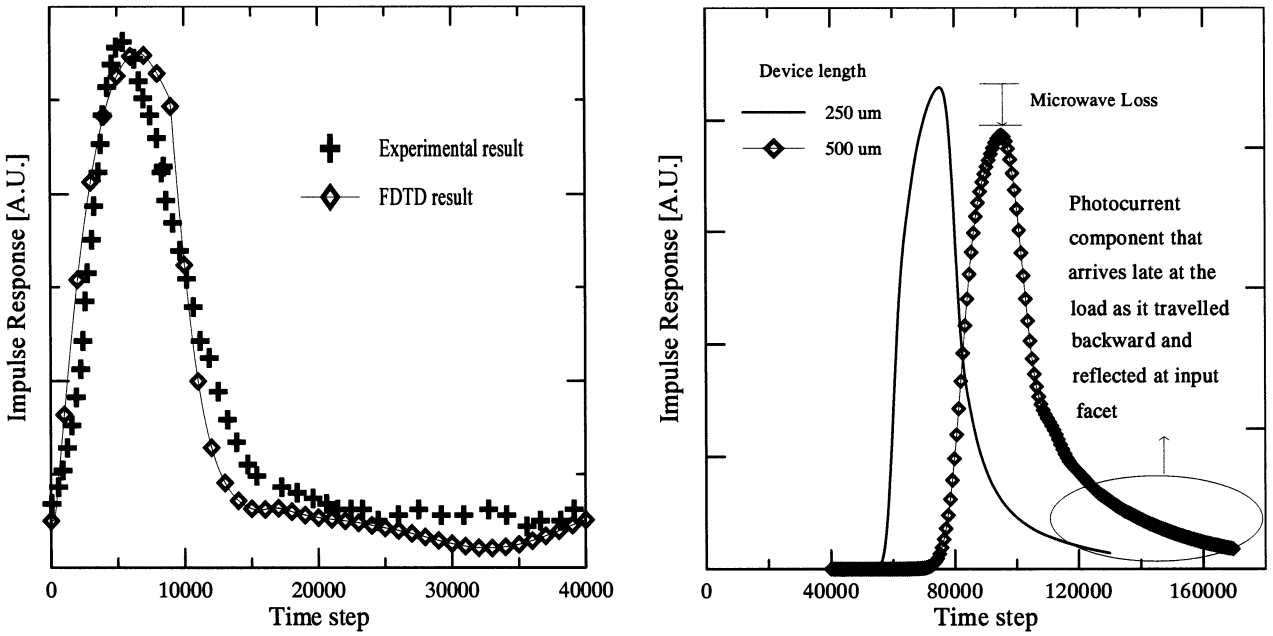

Fig. 9. Photocurrent at the output in the time domain. (a) Comparison of the experimental [17] and FDTD data. Impulse response of 1 (width) × 7 (length) μm^2 TWPD with 10.5 fC (linear regime) of photogenerated charge ($V_{\rm bias} = 1$ V, $\lambda = 830$ nm, TE illumination). (b) FDTD simulation of the impulse response with 250 and 500 μm of device length ($W_i = 3.0$ μm, $h = 1.0$ μm, time step $= 0.2$ fs).

achieved by an appropriate choice of those design parameters (around 2 μm of waveguide width).

Equations (5) and (6) are used in order to obtain microwave properties of TWPDs. $Z_{\rm open}$ and $Z_{\rm short}$ in (5) and (6) are frequency-domain data. Thus, by utilizing the time-domain response traces such as in Fig. 4, we obtained their corresponding Fourier transform data, as shown in Figs. 5–7 (FDTD result). The incident wave is a Gaussian pulse, and Fig. 4 depicts that the current wave with an open load and the voltage wave with a short load become out-of-phase at the termination, as expected. The distance (l) between the load and field observation point was 30 μm. Simulations in Figs. 5(a), 6(a), and 10(a) were executed with the waveguide width of 1.2 μm, and the i-region's thickness in Figs. 5(b), 6(b), and 10(b) was fixed at 1.4 μm. Simulations were executed for a typical case with the active i-region's thickness of 200 nm. Fig. 5 shows the field attenuation constant (α) as a variation of frequency. Microwave loss can be reduced with a thick i-layer and a narrow width of the waveguide.

RF refractive indexes are presented in Fig. 6. They are calculated from the value of effective permittivity and are closely related to the imaginary term of the propagation constant according to $n_{\rm eff}(f) = \sqrt{\varepsilon_{\rm eff}(f)\mu_r/\varepsilon_o}$ and $\varepsilon_{\rm eff}(f) = \sqrt{\beta^2(f)/\omega^2\mu_o}$. The microwave phase velocity is very low in the low frequency band, but it converges as the frequency goes up. This indicates that the microwave is dispersive only in the low-frequency band (below approximately 15 GHz in Fig. 6). Strictly speaking, however, this frequency point of criterion [the bending point of the curves in Figs. 3(b), 5–7(a)] may not be exact in fact because the FDTD method shows a dc offset [16] and also the HFSS has low-frequency limitation. The results of Fig. 6 represent that microwave speeds go up as the thickness of the i-layer gets thicker and the waveguide width gets narrower. As the transverse capacitance increases, the microwave phase velocity decreases. The capacitance is proportional to W_i/h. This basic principle agrees well with the result shown in Fig. 6. However, there is tradeoff in practical application because it is difficult to make a narrow waveguide width, and the thick core of the i-layer limits the bandwidth due to the carrier transit time and time delay is increased with the thick-cladding i layer.

Transmission characteristics by the two methods are compared in Fig. 7 to validate the simulation results for a fixed structure ($W_i = 3.0$ μm, $h = 1.0$ μm). The HFSS is a 3-D electromagnetic (EM) simulator, and only microwave characteristics are available from it. For the calculation of the impulse response, we modeled the signal source considering the optical wave field profile and carrier transit time for the space and time domains, respectively. The optical wave field distribution of waveguide in the xz-plane was obtained by applying the effective index method [14]. Fig. 8 presents the calculated optical field distribution in the intrinsic active region (core). These calculated data are applied to (4b) for source modeling, and (4a) and (4b) are related to the longitudinal and transverse directions, respectively. $J_z(y)$ is calculated from (4a) at any y-position and, in order to consider the carrier transit time, the optical wave field profile that is a function of the x- and z-position is applied into the FDTD code. As a result, the FDTD code with (4) enables us to obtain an impulse response considering the carrier transit time, optical field distribution, velocity mismatch, and microwave property.

Fig. 9 shows the impulse response in the time domain. To validate our simulation results, the linear impulse responses are compared with the experimental data in Fig. 9(a). The experimental response from [17] (GaAs–AlGaAs p-i-n graded double-heterostructure TWPD with 190 nm of de-

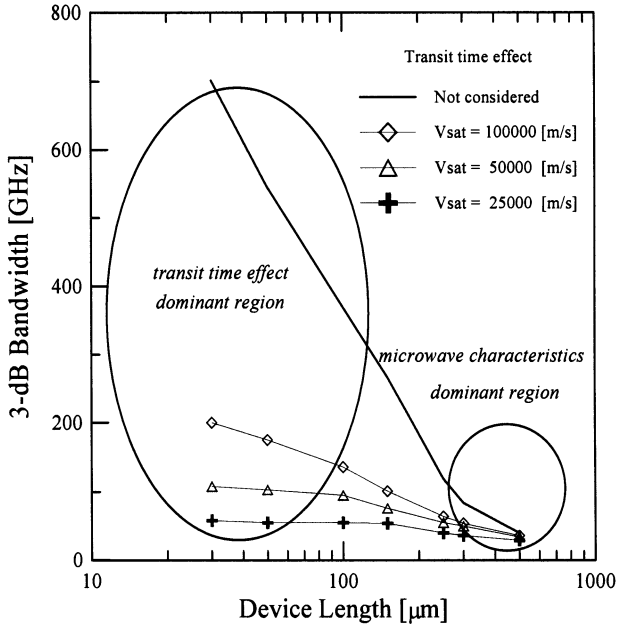

Fig. 10. Bandwidth of TWPDs according to the device length with and without considering the carrier transit time.

TABLE II
3-dB BANDWIDTH AND RF REFRACTIVE INDEX ACCORDING TO WAVEGUIDE GEOMETRY (DEVICE LENGTH $= 100\ \mu$m, $v_{\rm sat} = 0.5 \times 10^7$ cm/s)

Thickness of i-layer \ Waveguide width	1.2 μm	3.0 μm	4.8 μm
0.8 μm	97 GHz (3.54)	88 GHz (4.3)	84 GHz (4.76)
1.0 μm	99 GHz (3.23)	95 GHz (3.94)	87 GHz (4.35)
1.2 μm	102 GHz (3.0)	96 GHz (3.66)	90 GHz (4.05)
1.4 μm	106 GHz (2.83)	97 GHz (3.45)	93 GHz (3.82)

TABLE III
3-dB BANDWIDTH AND RF REFRACTIVE INDEX ACCORDING TO WAVEGUIDE GEOMETRY (DEVICE LENGTH $= 300\ \mu$m, $v_{\rm sat} = 0.5 \times 10^7$ cm/s)

Thickness of i-layer \ Waveguide width	1.2 μm	3.0 μm	4.8 μm
0.8 μm	56 GHz (3.54)	44 GHz (4.3)	39 GHz (4.76)
1.0 μm	61 GHz (3.23)	50 GHz (3.94)	41 GHz (4.35)
1.2 μm	67 GHz (3.0)	53 GHz (3.66)	44 GHz (4.05)
1.4 μm	71 GHz (2.83)	55 GHz (3.45)	48 GHz (3.82)

pletion-layer thickness) agrees well with that by our FDTD method ($\Delta y = 0.35\ \mu$m was used for this simulation). The photocurrents at the output are plotted with a device length of 250 and 500 μm in Fig. 9(b). It took 63 min/10 000 time steps for a personal computer (PC) (800-MHz Pentium III with 786-MB RAM on Windows 2000) to simulate the impulse response. More microwave loss is seen in the longer TWPD. The tails of the signal come from the fact that part of the photogenerated electrical wave arrives late at the load as it traveled backward and was reflected at the open input facet. After an impulse response of lightwave is calculated in the time domain with a fixed light absorption ($\alpha_0 = 1000\ \text{cm}^{-1}$), it is Fourier transformed to obtain the frequency response.

The impulse response is obtained as follows. Δy is set to device length/15 with 59 mesh dimensions in the y-direction. For example, when the device length is 150 μm, Δy is set to 10 μm. The impulse response is calculated at the position that is 15 grids away from the input end. During the simulation, the wave travels forward and, at the output, reflection (error by ABC) occurs. However, the reflection cannot reach the observation point before the simulation ends. Thus, we obtain the impulse response exactly without any reflection from the output end.

Fig. 10 shows an interesting example, i.e., how the transit time and microwave characteristics have an effect on the bandwidth. Here, it is assumed that the TWPD operates at a linear regime, and the active i-layer has 0.2-μm thickness. The saturation velocity of photogenerated carriers under reverse dc bias was assumed to be ∞, 10^7, 0.5×10^7, and 0.25×10^7 cm/s in the simulation. Although the saturation velocity is close to 0.5×10^7 cm/s in practice, the results with various values of $v_{\rm sat}$ are given for the purpose of bandwidth analysis. Here, the waveguide width is 3.0 μm and the thickness of the i-layer is 1.0 μm.

If the device length is shorter than 300–500 μm, 3-dB bandwidth is dominated by carrier transit time effect. However, it is limited by microwave features when the device length is much longer because the values of 3-dB bandwidth converge irrespective of the transit time. Consequently, the dominant bandwidth limiting factor depends on the TWPD's length. The transit time affects more bandwidth with increasing transit time, and there exists a bandwidth limitation, however short the device length is. It is an important problem to find out the optimal waveguide length for the high bandwidth-efficiency product and good linearity, although they are beyond the scope of this paper. On the other hand, the objective of this paper is to analyze the bandwidth limitation considering the microwave loss, dispersion, and the velocity mismatch. It is observed in Figs. 5 and 6 that the deeper i-layer or narrower waveguide makes better microwave property. Thus, it should be underlined that low microwave loss or low RF refractive index enhances 3-dB bandwidth and that the tendencies of bandwidth limitation and microwave characteristics according to the design parameters are coincident (Tables II and III). It is noticeable that if input ter-

minal is open, bandwidth is proportional to microwave phase velocity, and it is very important how well velocity is matched only in the case of an impedance matched input port [7]. The simulation results in Tables II and III correspond to it. Tables II and III show 3-dB bandwidth and an RF refractive index $(n_{\rm rf})$. In terms of device design, narrow waveguide is required, but it would be a tradeoff with the possibility of fabrication. When the waveguide width is reduced from 4.8 to 1.2 μm, the bandwidth is strongly increased by more than 40% in case that device length is 300 μm. With device length of 100 μm, the FDTD simulation shows approximately 106 GHz of bandwidth when the thickness and width are 1.4 and 1.2 μm, respectively.

IV. Conclusion

We have developed a numerical modeling tool by applying a 3-D FDTD method for investigating the effects on bandwidth of TWPDs. Full-wave analysis in this paper is very meaningful as follows. First, all the geometry and material have been incorporated into the numerical technique. Second, impulse response has been calculated, taking into account at once the optical field distribution, carrier transit time, microwave loss, dispersion, and velocity mismatch. The thickness of the i-layer and waveguide width has been used as design parameters, and it has been shown how these parameters contribute to the microwave characteristics and 3-dB bandwidth. We have obtained bandwidth of 106 GHz with a fixed device length of 100 μm for 1.4-μm i-layer's thickness and 1.2-μm waveguide width. We have also shown that there exists a dominant factor for bandwidth limitation according to the TWPD's length.

References

[1] J. Soohoo, S. K. Yao, J. E. Miller, R. R. Shurtz, II, Y. Taur, and R. A. Gudmundsen, "A laser-induced traveling-wave device for generating millimeter waves," *IEEE Trans. Microwave Theory Tech.*, vol. MTT-29, pp. 1174–1182, Nov. 1981.

[2] H. F. Taylor, O. Eknpyan, C. S. Park, K. N. Choi, and K. Chang, "Traveling-wave photodetectors," *Proc. SPIE—Int. Soc. Opt. Eng.*, vol. 1217, pp. 59–63, 1990.

[3] R. J. Deri, "Monolithic integration of optical waveguide circuitry with photodetectors for advanced lightwave receivers," *J. Lightwave Technol.*, vol. 11, pp. 1296–1313, Aug. 1993.

[4] D. Wake, "A 1550-nm millimeter-wave photodetector with a bandwidth-efficiency product of 2.4 THz," *J. Lightwave Technol.*, vol. 10, pp. 908–912, July 1992.

[5] K. S. Giboney, M. J. W. Rodwell, and J. E. Bowers, "Traveling-wave photodetectors," *IEEE Photon. Technol. Lett.*, vol. 4, pp. 1363–1365, Dec. 1992.

[6] V. M. Hietala and G. A. Vawter, "A large-bandwidth high-quantum efficiency traveling-wave photodetector based on a slow-wave coplanar transmission line," presented at the Electromagnetics Res. Symp., Cambridge, MA, July 1991.

[7] K. S. Giboney, M. J. W. Rodwell, and J. E. Bowers, "Traveling-wave photodetector theory," *IEEE Trans. Microwave Theory Tech.*, vol. 45, pp. 1310–1319, Aug. 1997.

[8] K. S. Yee, "Numerical solution of initial boundary value problems involving Maxwell's equations in isotropic media," *IEEE Trans. Antennas Propagat.*, vol. MTT-14, pp. 302–307, May 1966.

[9] S. M. El-Ghazaly, R. P. Joshi, and R. O. Grondin, "Electromagnetic and transport considerations in subpicosecond photoconductive switch modeling," *IEEE Trans. Microwave Theory Tech.*, vol. 38, pp. 629–637, May 1990.

[10] E. Sano and T. Shibata, "Fullwave analysis of picosecond photoconductive switches," *IEEE J. Quantum Electron.*, vol. 26, pp. 372–377, Sept. 1990.

[11] A. Taflove and M. E. Brodwin, "Numerical solution of steady-state electromagnetic scattering problems using the time-dependent Maxwell's equations," *IEEE Trans. Microwave Theory Tech.*, vol. MTT-23, pp. 623–630, MONTH 1975.

[12] G. Mur, "Absorbing boundary conditions for the finite-difference approximation of the time-domain electromagnetic field equations," *IEEE Trans. Electromagn. Compat.*, vol. EMC-23, pp. 377–381, MONTH 1981.

[13] K. Kato, "Ultrawide-band/high-frequency photodetectors," *IEEE Trans. Microwave Theory Tech.*, vol. 47, pp. 1265–1281, July 1999.

[14] C. Pollock, *Fundamentals of Optoelectronics*. Homewood, IL: Irwin, 1995, pp. 49–74 215–240.

[15] G. C. Liang, Y. W. Liu, and K. K. Mei, "Full-wave analysis of coplanar waveguide and slotline using the time-domain finite-difference method," *IEEE Trans. Microwave Theory Tech.*, vol. 37, pp. 1949–1957, Dec. 1989.

[16] C. M. Furse, D. H. Roper, D. N. Buechler, D. A. Christensen, and C. H. Durney, "The problem and treatment of DC offsets in FDTD simulations," *IEEE Trans. Antennas Propagat.*, vol. 48, pp. 1198–1201, Aug. 2000.

[17] K. S. Giboney, M. J. W. Rodwell, and J. E. Bowers, "Traveling-wave photodetector design and measurements," *IEEE J. Select. Topics Quantum Electron.*, vol. 2, pp. 622–629, Sept. 1996.

Soon-Cheol Kong was born in Youngwol, Korea, on May 12, 1971. He received the B.S. and M.S. degrees in electronic engineering from Chung-Ang University, Seoul, Korea, in 1995 and 1997, respectively, and is currently working toward the Ph.D. degree at Chung-Ang University.

His research interests include FDTD simulation, antenna design, and opto-electronic devices.

Seung-Jin Lee was born in Seoul, Korea, on May 3, 1972. He received the B.S. degree in electronic engineering and M.S. degree in image engineering from Chung-Ang University, Seoul, Korea in 1999 and 2001, respectively.

Since 2001, he has been with Samsung Electronics, Suwon, Korea. His research interests include optical network systems and opto-electronic devices.

Jung-Hoon Lee was born in Mokpo, Korea, on February 12, 1977. He received the B.S. degree in electronic engineering and M.S. degree in image engineering from Chung-Ang University, Seoul, Korea in 1999 and 2001, respectively.

Since 2001, he has been with Blue Stellar Wave (BSW), Inchon, Korea. His research interests include optical repeater and opto-electronic devices.

Young-Wan Choi (S'90–M'92) received the B.S. degree in electronic engineering from Sogang University, Seoul, Korea, in 1985, and the M.S. and Ph.D. degree in electrical and computer engineering from the State University of New York at Buffalo, in 1987 and 1992, respectively.

From 1992 to 1995, he was a Senior Researcher with the Electronics and Telecommunications Research Institute, Daejeon, Korea, where he conducted research on optical switching devices such as self-electrooptic effect devices and electro-absorptioin modulators. In 1995, he joined the Department of Electronic Engineering, Chung-Ang University, Seoul, Korea, where he is currently a Professor. He has authored over 90 research papers in various international journals and conference proceedings. His research interests are microwave photonics, optical switching devices, and optical interconnects.